Research Square

Preprints are preliminary reports that have not undergone peer review.
They should not be considered conclusive, used to inform clinical practice,
or referenced by the media as validated information.

Secondary-Path-Compensated FxLMS Active Control of Milling Chatter in Thin-Walled Workpieces

Zicheng Wang
Cheng Wang
Benchi Zhu
Wenbo He
Mingjie Cai
Guolong Zhao
Yinfei Yang
yyfgoat@nuaa.edu.cn

Nanjing University of Aeronautics and Astronautics

Research Article

Keywords: thin-walled workpiece, milling chatter, active vibration control, filtered-x least-mean-square algorithm, secondary-path compensation, piezoelectric stack actuator

Posted Date: November 18th, 2026

DOI: https://doi.org/10.21203/rs.3.rs-10982997/v1

License: This work is licensed under a Creative Commons Attribution 4.0 International License.
Read Full License

Secondary-Path-Compensated FxLMS Active Control of Milling Chatter in Thin-Walled Workpieces

Zicheng Wang · Cheng Wang · Benchi Zhu · Wenbo He · Mingjie Cai · Guolong Zhao · Yinfei Yang*

College of Mechanical and Electrical Engineering, Nanjing University of Aeronautics and Astronautics, Nanjing 210016, China

Corresponding author: Yinfei Yang | E-mail: yangyf@nuaa.edu.cn

Acknowledgements: This work was supported by the Fundamental Research Funds for the Central Universities (Grant No. NG2024013).

Abstract

Thin-walled workpieces are vulnerable to narrow-band milling chatter because of their low local stiffness and time-varying structural dynamics. In a piezoelectric active-control system, the controller output reaches the acceleration measurement point through the piezoelectric controller, stack actuator, plate structure, and sensing chain. The gain, phase, and delay of this physical secondary path can bias the weight-update direction of a conventional least-mean-square (LMS) controller. This study therefore develops a filtered-x least-mean-square (FxLMS) method that uses an equivalent control-force-to-acceleration model as the secondary-path estimate to prefilter the reference signal. The method is implemented on a 6061 aluminium-alloy plate (300 mm × 300 mm × 4 mm) supported at its four corners with a piezoelectric stack actuator and one acceleration measurement channel. It is evaluated using an LMS/FxLMS simulation under identical conditions, offline simulations driven by measured milling signals, and comparative milling tests. With a total delay of 0.8 ms, LMS reduces the steady-state root-mean-square (RMS) response by 8.1% and amplifies the 558.857 Hz component, whereas FxLMS reduces the RMS response by 82.9% and attenuates both target components. In milling tests at 4000, 7000, and 10000 r/min, vibration amplitudes decrease by approximately 75.0%, 66.7%, and 50.0%, while arithmetic mean surface roughness (Ra) decreases by 65.6%, 53.6%, and 15.6%, respectively. The results indicate that secondary-path compensation provides a low-complexity, implementable route for active chatter suppression on the investigated thin-plate milling platform, while the reduced high-speed benefit identifies the limitation of a fixed secondary-path estimate.

Keywords: thin-walled workpiece; milling chatter; active vibration control; filtered-x least-mean-square algorithm; secondary-path compensation; piezoelectric stack actuator

1 Introduction

Thin-walled components are widely used in aerospace structures because of their high specific strength and low mass. Their low local stiffness, however, makes them susceptible to regenerative chatter during milling. Chatter not only enlarges vibration and cutting-force fluctuations but also degrades surface integrity, accelerates tool wear, and limits attainable material-removal rates. Existing suppression strategies can be broadly classified as passive, semi-active, and active approaches. Passive damping devices are structurally simple but are usually tuned to a limited frequency range; semi-active methods offer adjustable dynamic properties but still depend on a prescribed actuation mechanism. Active methods use measured vibration to generate a counteracting force and are therefore attractive when the dominant chatter band and structural response vary during machining [1–5].

Previous studies have demonstrated several active-control routes. Auxiliary damping devices, adjustable fixtures, and piezoelectric devices have been investigated for structural or machining vibration suppression [6–15]. Fuzzy, modal, and adaptive control approaches have been studied for these applications [11,13–15,24]. These studies establish that active actuation can improve machining stability, but the suitability of a controller depends strongly on sensing topology, actuator dynamics, available computation, target-frequency concentration, and model uncertainty. For the platform considered here, the

dominant chatter components are concentrated near 180 and 560 Hz, only one acceleration channel is available for vibration measurement, and the controller must update at 2500 Hz. A low-order adaptive controller is consequently preferable to a large state-space model or a computationally intensive online optimiser.

The conventional least-mean-square (LMS) algorithm is attractive because of its small computational burden and online adaptation capability. It updates the filter weights directly from a reference signal and the residual error. In the present piezoelectric control chain, however, the controller output does not act directly at the measurement point. It passes through the piezoelectric controller, the PSt150 stack actuator, the thin plate, and the acceleration-sensing chain. This physical secondary path introduces frequency-dependent gain, phase shift, and delay. If these dynamics are omitted from the gradient estimate, LMS may update its weights in a direction that is inconsistent with the actual residual response, so that one target component is attenuated while another is amplified [22,23].

The filtered-x least-mean-square (FxLMS) algorithm addresses this specific problem by filtering the reference signal through a secondary-path estimate before calculating the adaptive update. FxLMS has been widely used in active noise and structural-vibration control because it retains the low computational cost of LMS while accounting for the actuator-to-sensor path [11,14,22–24]. Its role in the present work is therefore not to claim universal superiority over all active-control methods. Rather, its modelling assumptions and computational requirements match the investigated narrow-band, single-channel piezoelectric milling platform: the dominant chatter bands can be extracted from acceleration data, a compact secondary-path model can represent the control-force-to-measured-acceleration relation, and the weights can be updated online at the available sampling rate.

Signal-based chatter-monitoring methods provide the basis for distinguishing chatter from other machining responses [5,16–21]. Chatter identification and active suppression are treated as two connected but distinct functions. A previously developed convolutional neural network–long short-term memory (CNN–LSTM) model provides chatter-state identification, while the ratio of chatter-band energy to total selected-band energy provides the control trigger [25]. Once control is enabled, FxLMS generates the compensating signal. The present study focuses on the secondary-path-induced mismatch and its correction rather than retraining the identification model.

Accordingly, this study asks how the amplitude, phase, and delay of the actual secondary path affect an LMS controller for thin-plate milling, and whether secondary-path prefiltering can correct the weight-update direction without sacrificing low computational complexity. The main contributions are: (1) an experimentally grounded definition of the complete controller–actuator–plate–sensor secondary path; (2) an equivalent control-force-to-acceleration model used for FxLMS reference prefiltering; (3) a unified identification–triggering–control chain for the investigated platform; and (4) validation by simulation under identical conditions, measured-signal offline simulation, and comparative milling tests at three spindle speeds.

2 Experimental system and secondary-path modelling

2.1 Platform and dynamic parameters

The active-control system is built around a NINGQING VC-1060 vertical machining centre and consists of the workpiece fixture, vibration measurement, piezoelectric actuation, and control-computing modules. Figure 1 shows the platform configuration. The pressure sensor is used only for actuator preload monitoring and load calibration; it is not treated as the reference or error sensor for chatter control.

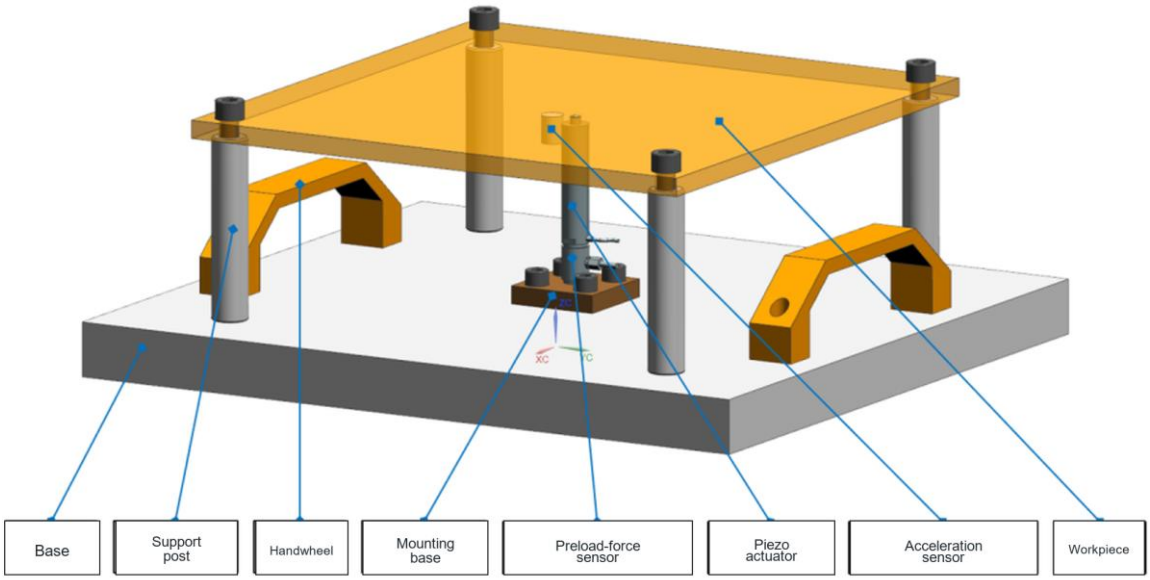


Fig. 1 Schematic of the thin-plate milling active-control platform

The research object is a 6061 aluminium-alloy plate with dimensions of 300 mm × 300 mm × 4 mm. Four 304 stainless-steel posts provide corner support to reproduce a locally flexible plate boundary while retaining a controllable and repeatable laboratory configuration. The experimental platform is shown in Fig. 2. A 1A119E accelerometer is mounted on the sensitive region of the plate underside; its range is ±50 g and its frequency range is 0.5–12000 Hz. The signal is conditioned through an IEPE unit and sampled at 2500 Hz. A PSt150/10/60 VS15 piezoelectric stack actuator is installed near the plate centre with its output direction aligned with the acceleration measurement direction. The control voltage is amplified by a piezoelectric controller before driving the actuator.

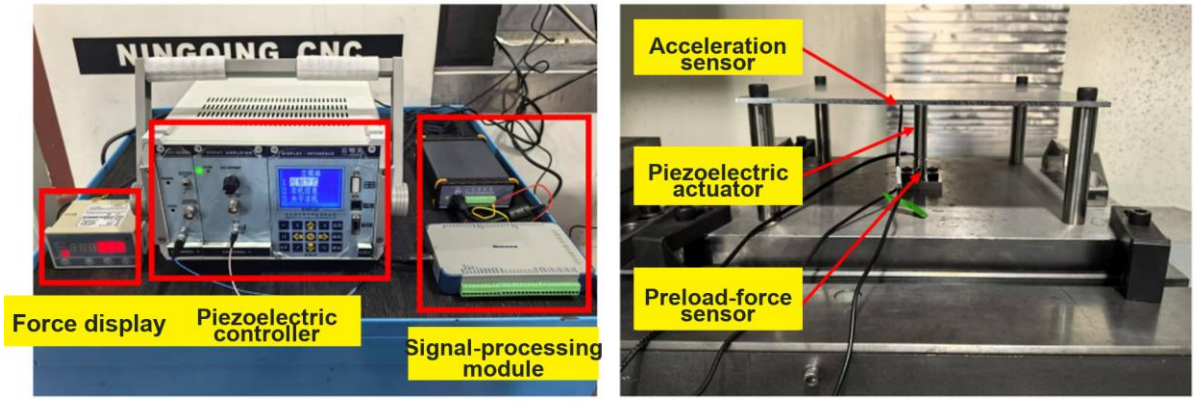


Fig. 2 Experimental platform and principal sensing/actuation components

Table 1 Main parameters of the piezoelectric stack actuator

Parameter	Value
Nominal travel	57 μm
Stiffness	35 N/μm
Push/pull force	2300/500 N
Capacitance	11 μF
Resonant frequency	14 kHz
Length	64 mm

During operation, the same accelerometer continuously records the plate response. Target-band historical samples form the reference branch x(n), while the current residual acceleration after piezoelectric

action forms the error signal e(n). These signals are distinguished by time indexing and algorithmic function rather than by duplicating the physical sensor. This single-sensor history-based arrangement reflects the actual platform and avoids implying an uninstalled feedforward reference sensor.

2.2 Equivalent secondary-path model

For adaptive-control design, the local plate response in the two target bands is approximated by a single-degree-of-freedom equivalent model. This approximation is not intended to reproduce the complete multimodal behaviour of an arbitrary thin-walled part. Its purpose is to provide a calculable bridge for the target-band chain from control force, through structural propagation, to measured acceleration. The plate flexural rigidity is

$$D = Et^3/[12(1-\nu^2)] \tag{1}$$

where E = 69 GPa is the elastic modulus, t = 0.004 m is the plate thickness, and ν = 0.33 is Poisson's ratio. Equation (1) gives D = 412.97 N·m. The equivalent plate stiffness is estimated as

$$k_{plate} = \alpha_k D/a^2 \tag{2}$$

where a = 0.3 m is the plate side length and α_k = 0.0399 is a dimensionless coefficient that accounts for four-corner support, the equivalent mode shape, and the measurement location. The resulting equivalent stiffness is approximately 183 N/m. The axial stiffness of each support post is

$$k_{support} = EA/L \tag{3}$$

For a 10 mm diameter, 100 mm long steel post with E = 210 GPa, the axial stiffness is 1.65×10^8 N/m, which is much larger than the equivalent plate stiffness:

$$k_{support} \gg k_{plate} \tag{4}$$

Support deformation is therefore neglected in the target-band equivalent model. The plate equivalent mass is

$$m = \rho A t \tag{5}$$

With ρ = 2700 kg/m³, A = 0.3 × 0.3 m², and t = 0.004 m,

$$m = 0.972 \text{ kg} \tag{6}$$

Using an engineering damping ratio ζ = 0.02, the equivalent viscous damping coefficient is

$$c = 2\zeta\sqrt{(mk_{plate})} \tag{7}$$

$$c = 0.534 \text{ N·s/m} \tag{8}$$

The equivalent dynamics are consequently defined by m = 0.972 kg, k_{plate} = 183 N/m, and c = 0.534 N·s/m. These parameters support secondary-path modelling and controller comparison; they are not presented as a complete modal characterisation of the plate.

Let w(t) denote the plate displacement associated with the equivalent target-band response and F(t) the piezoelectric control force. The governing equation is

$$m\ddot{w}(t) + c\dot{w}(t) + k_{plate}w(t) = F(t) \tag{9}$$

Under zero initial conditions, its Laplace-domain form is

$$ms^2X(s) + csX(s) + k_{plate}X(s) = F(s) \tag{10}$$

$$X(s) = F(s)/(ms^2 + cs + k_{plate}) \tag{11}$$

Because acceleration is the measured quantity,

$$\ddot{w}(t) \leftrightarrow s^2X(s) \tag{12}$$

and the continuous transfer function from control force to measured acceleration is

$$H(s) = s^2/(ms^2 + cs + k_{plate}) \tag{13}$$

$$H(s) = s^2/(0.972s^2 + 0.534s + 183) \tag{14}$$

A bilinear transform is applied using

$$s = (2/T)(z - 1)/(z + 1) \tag{15}$$

At f_s = 2500 Hz (T = 0.0004 s), the discrete secondary-path estimate becomes

$$H(z) = (1.028686z^2 - 2.057372z + 1.028686)/(z^2 - 1.999750z + 0.999780) \tag{16}$$

In the controller, this low-order model is denoted by $\hat{S}(z)$. It represents the dominant target-band dynamics of the physical secondary path S(z) and is used only to prefilter the reference signal for weight updating. Model uncertainty remains unavoidable; the experiments therefore evaluate whether the estimate is sufficiently accurate for the investigated platform rather than claiming exact identification of the complete physical chain.

3 FxLMS active-control method

3.1 LMS mismatch and secondary-path compensation

For an M-tap adaptive filter, the reference vector is

$$x(n) = [x(n), ..., x(n - M + 1)]^T \tag{17}$$

The controller output is

$$y(n) = w^T(n)x(n) \tag{18}$$

where w(n) is the adaptive-weight vector. In an idealised LMS formulation, the error and weight update are

$$e(n) = d(n) - y(n) \tag{19}$$

$$w(n + 1) = w(n) + \mu e(n)x(n) \tag{20}$$

This formulation implicitly assumes that y(n) acts at the error point without additional dynamics. In the physical system, however, the controller output is transmitted through S(z). The measured control contribution is

$$y_s(n) = S(z)\cdot y(n) \tag{21}$$

and the actual residual is

$$e(n) = d(n) - y_s(n) \tag{22}$$

The amplitude response, phase response, and delay of S(z) directly affect the residual gradient. Updating the weights with the unfiltered reference x(n) therefore gives a biased gradient estimate. In a multi-frequency case, this mismatch can attenuate one component while increasing another.

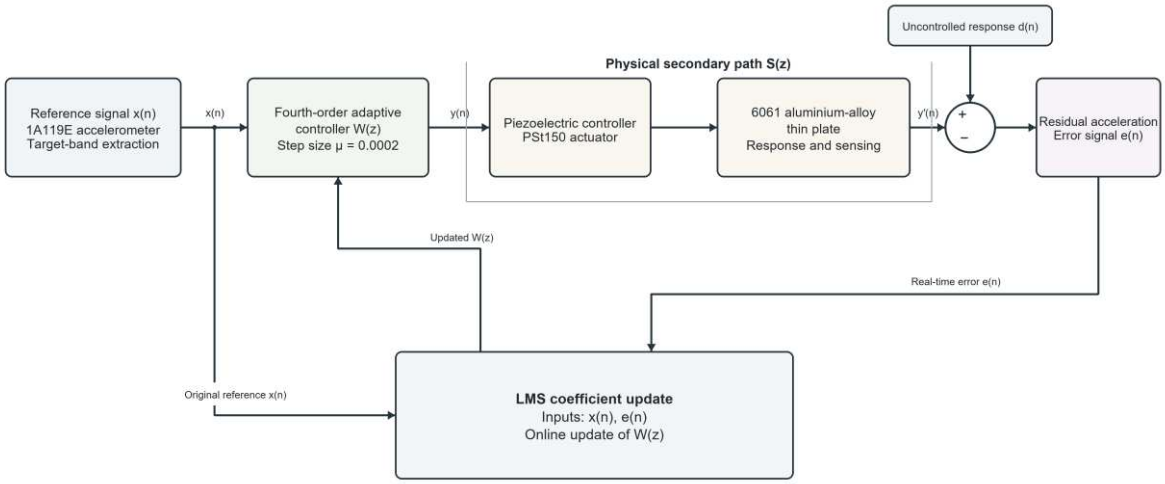
FxLMS preserves the adaptive filter of LMS but introduces the secondary-path estimate $\hat{S}(z)$. The filtered reference is

$$\hat{x}(n) = \hat{S}(z)\cdot x(n) \tag{23}$$

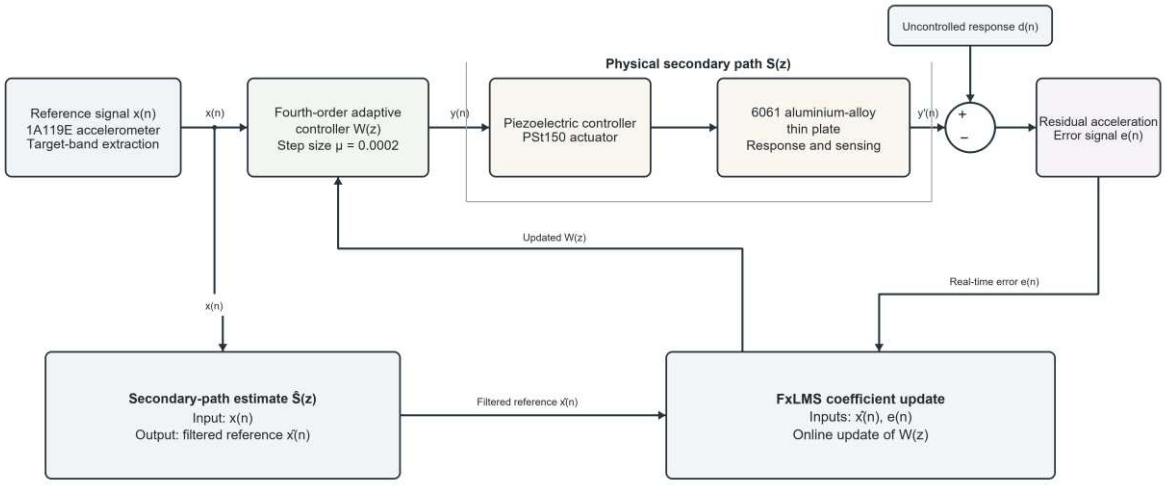
and the weight update becomes

$$w(n + 1) = w(n) + \mu e(n)\hat{x}(n) \tag{24}$$

The compensation does not remove the physical secondary path. Instead, it incorporates an estimate of that path into the gradient calculation so that the update direction more closely represents the effect of control at the acceleration measurement point. Figures 3(a) and 3(b) compare the conventional LMS and FxLMS structures.



(a) Conventional LMS



(b) FxLMS

Fig. 3 Active-control structures: (a) conventional LMS; (b) secondary-path-compensated FxLMS

3.2 Signal chain and triggering logic

Figure 4 summarises the sensing, identification, triggering, and control chain implemented on the platform. The 1A119E accelerometer signal is conditioned and sampled at 2500 Hz. Band-pass filters extract 170–190 Hz and 550–570 Hz components, which cover the dominant bands identified from the measured spectra. Historical target-band samples form x(n); the current controller output y(n) is amplified and applied through the PSt150 actuator; and the residual acceleration at the same measurement point forms e(n). The FxLMS update uses the pair $\hat{x}(n)$, e(n), where $\hat{x}(n)$ is obtained from the estimated secondary path.

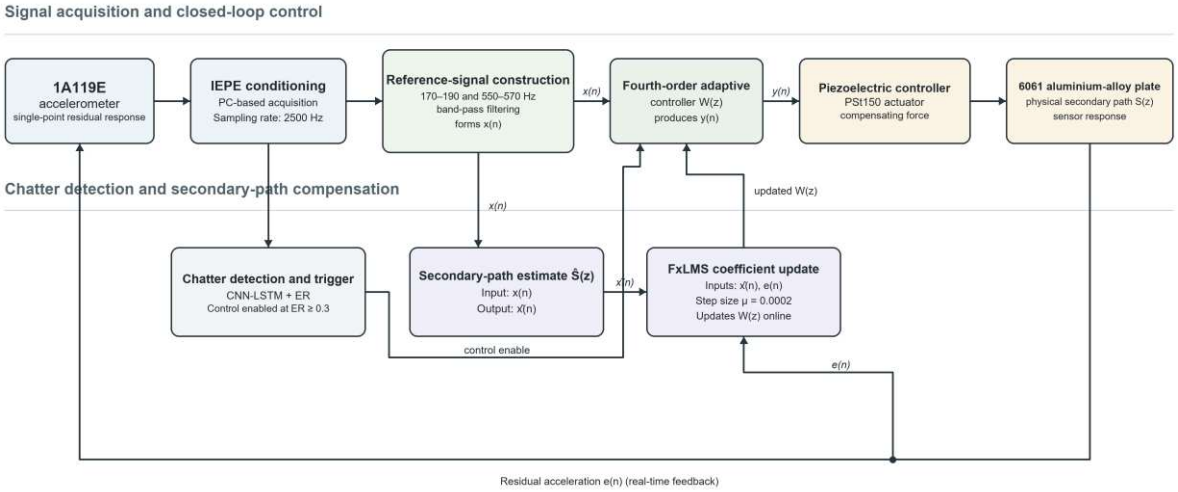


Fig. 4 FxLMS signal-processing and active-control chain on the experimental platform

Continuous actuation would increase energy consumption and may introduce unnecessary excitation when chatter is absent. A CNN–LSTM model is therefore used for chatter-state identification, while a frequency-domain energy ratio provides the control trigger. Let E_c denote the energy in the selected chatter bands and E_p denote the remaining energy within the evaluated spectral range. The trigger variable is

$$\mathrm{ER} = E_c/(E_c + E_p) \tag{25}$$

$$\mathrm{ER} \geq 0.3 \Rightarrow \text{control enabled} \tag{26}$$

$$\mathrm{ER} < 0.3 \Rightarrow \text{control disabled} \tag{27}$$

The previously trained CNN–LSTM classifier reported a test accuracy of 97.3% for the available dataset [25]. In the present study, that result is used as the state-identification input; the identification network is not retrained or claimed as a new contribution. The controller is activated only when the classifier and the energy-ratio trigger indicate chatter, thereby separating state recognition from adaptive suppression.

3.3 Controller parameters

The adaptive controller uses four taps and a sampling frequency of 2500 Hz. The two target bands are 170–190 Hz and 550–570 Hz. A small step size is selected to maintain stable online adaptation:

$$\mu = 0.0002 \tag{28}$$

The same filter order, step size, reference signal, and disturbance input are used in the LMS/FxLMS comparison so that the effect of secondary-path compensation can be isolated. Practical output limiting is applied according to the piezoelectric controller and actuator capability.

4 Simulation and experimental validation

4.1 LMS/FxLMS simulation under identical conditions

A two-frequency disturbance containing 181.571 and 558.857 Hz components is used to compare LMS and FxLMS under identical conditions. Both controllers use the same disturbance, initial weights, filter order, and step size. The simulation includes a total delay of 0.8 ms in the secondary path. Figure 5 presents the steady-state time response, Fig. 6 presents the sliding-RMS convergence process, and Fig. 7 compares the steady-state spectra.

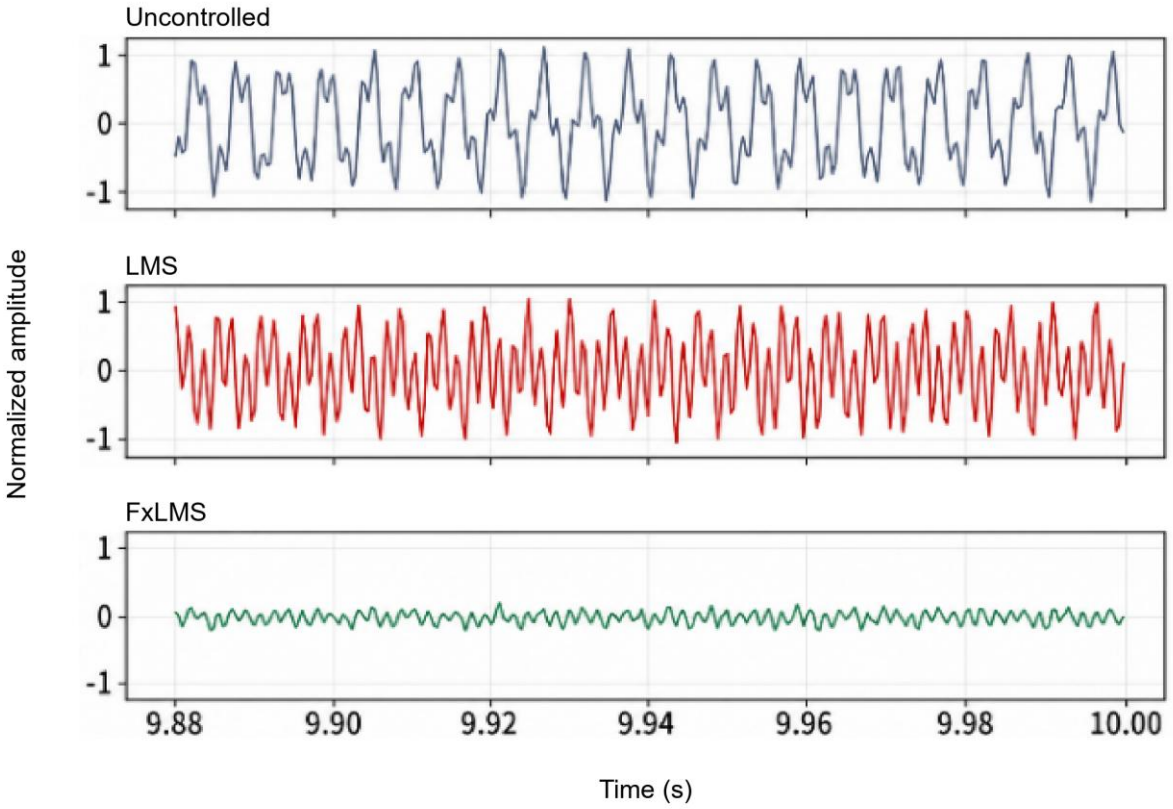


Fig. 5 Steady-state time responses for the uncontrolled, LMS-controlled, and FxLMS-controlled cases

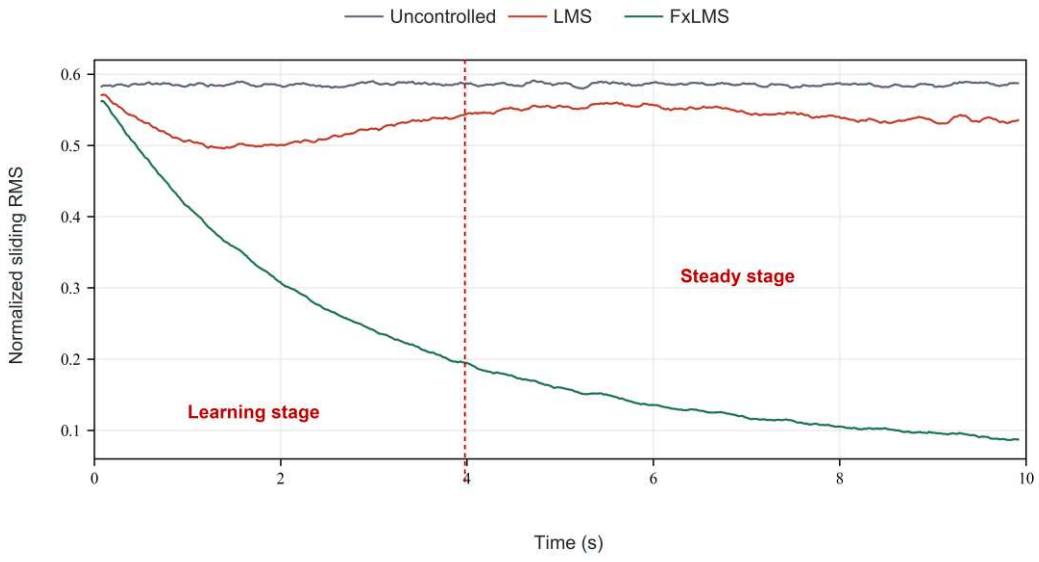


Fig. 6 Sliding-RMS convergence process. The initial period of approximately 4 s represents the adaptive-learning stage; the subsequent interval represents the relatively steady stage

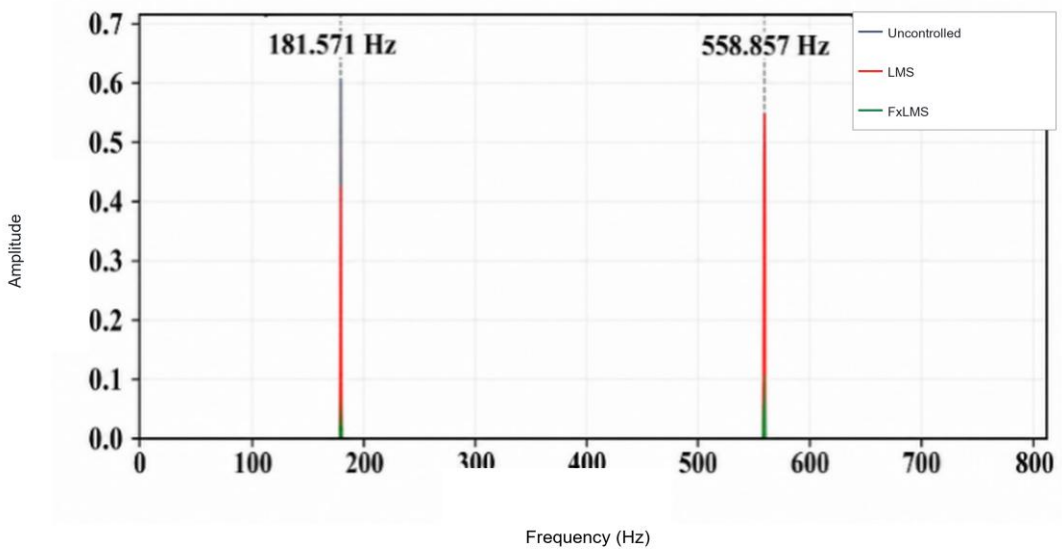


Fig. 7 Steady-state spectral comparison for LMS and FxLMS control

The approximately 4 s boundary in Fig. 6 separates two behaviours rather than indicating that weight updating stops. During the learning stage, the adaptive filter begins from its initial weights and FxLMS repeatedly prefilters the reference through $\hat{S}(z)$ before correcting the weights from the residual error. After approximately 4 s, the weights enter a relatively stable range and the control effect becomes consistent with steady machining. FxLMS nevertheless continues to update online throughout the steady stage.

Table 2 LMS and FxLMS simulation results under identical conditions

Condition	Steady-state RMS	RMS reduction	181.571 Hz amplitude	558.857 Hz amplitude
Uncontrolled	0.5850	0%	0.6851	0.3510
LMS	0.5377	8.1%	0.4250	0.5576
FxLMS	0.1000	82.9%	0.0576	0.1061

Conventional LMS reduces the steady-state RMS by only 8.1%. Although the 181.571 Hz component decreases, the 558.857 Hz component increases from 0.3510 to 0.5576. This is the multi-frequency imbalance expected when the physical secondary path is omitted from the gradient estimate. FxLMS reduces the RMS by 82.9% and lowers both target components to 0.0576 and 0.1061, corresponding to reductions of 91.6% and 69.8%. The comparison supports the specific role of secondary-path prefiltering: it corrects the update direction under the modelled amplitude, phase, and delay conditions. It does not, by itself, establish superiority over every possible active-control strategy.

4.2 Offline simulation driven by measured milling signals

To evaluate the method with nonstationary machining data, previously measured milling acceleration signals are used as offline inputs. These data are processed by the band-pass filters and the FxLMS control model shown in Fig. 8. The purpose differs from Section 4.1: the simulation under identical conditions isolates the influence of secondary-path compensation, whereas this stage tests whether the control chain remains effective for measured signals containing changes in speed, frequency, and chatter intensity.

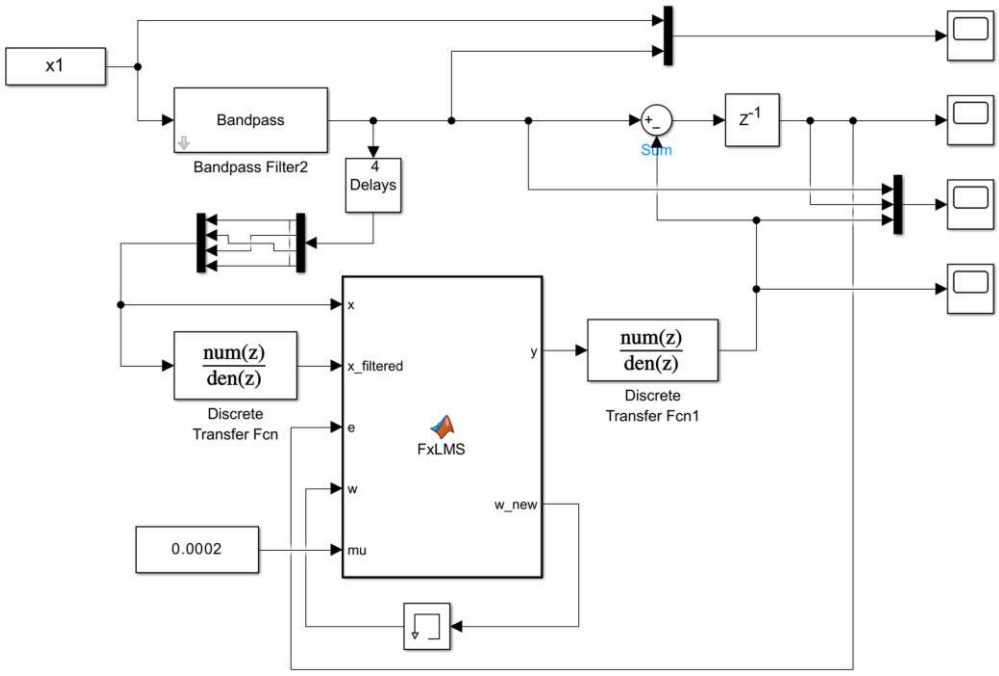


Fig. 8 Overall offline simulation model

The model uses a sampling frequency of 2500 Hz, a fourth-order controller, μ = 0.0002, and reference bands near 180 and 560 Hz. Figure 9 compares the measured signal before and after target-band filtering. Figure 10 presents an example before/after FxLMS signal, and Fig. 11 compares offline suppression for three spindle-speed conditions.

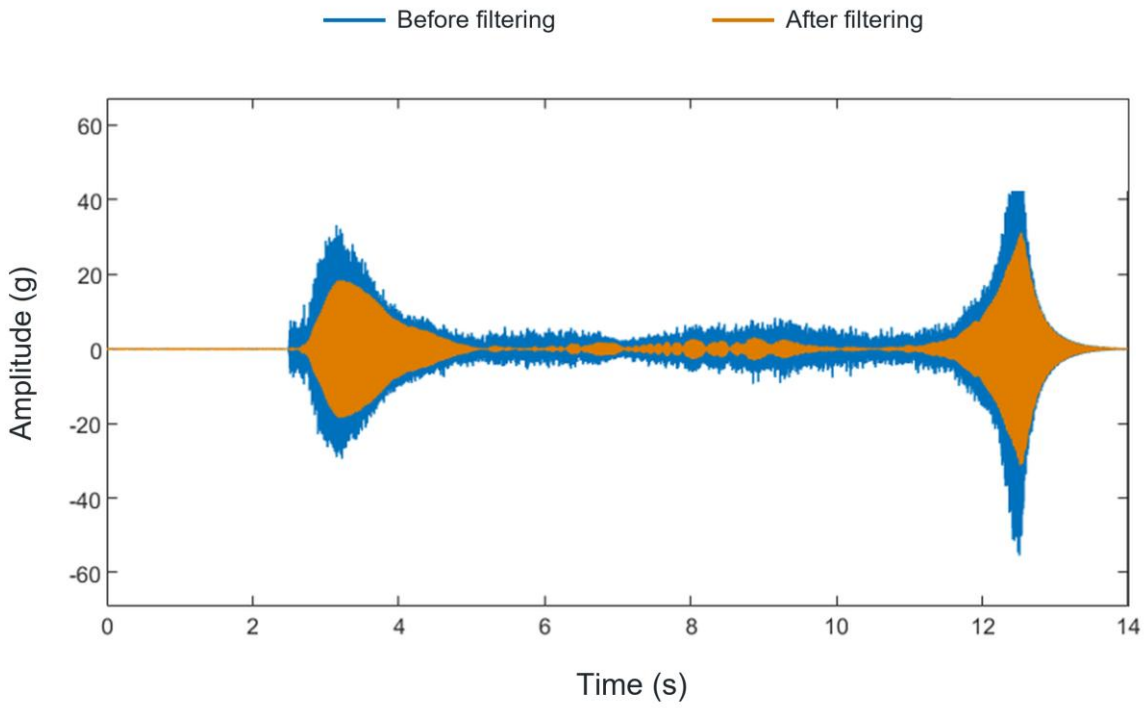


Fig. 9 Comparison of the measured signal before and after target-band filtering

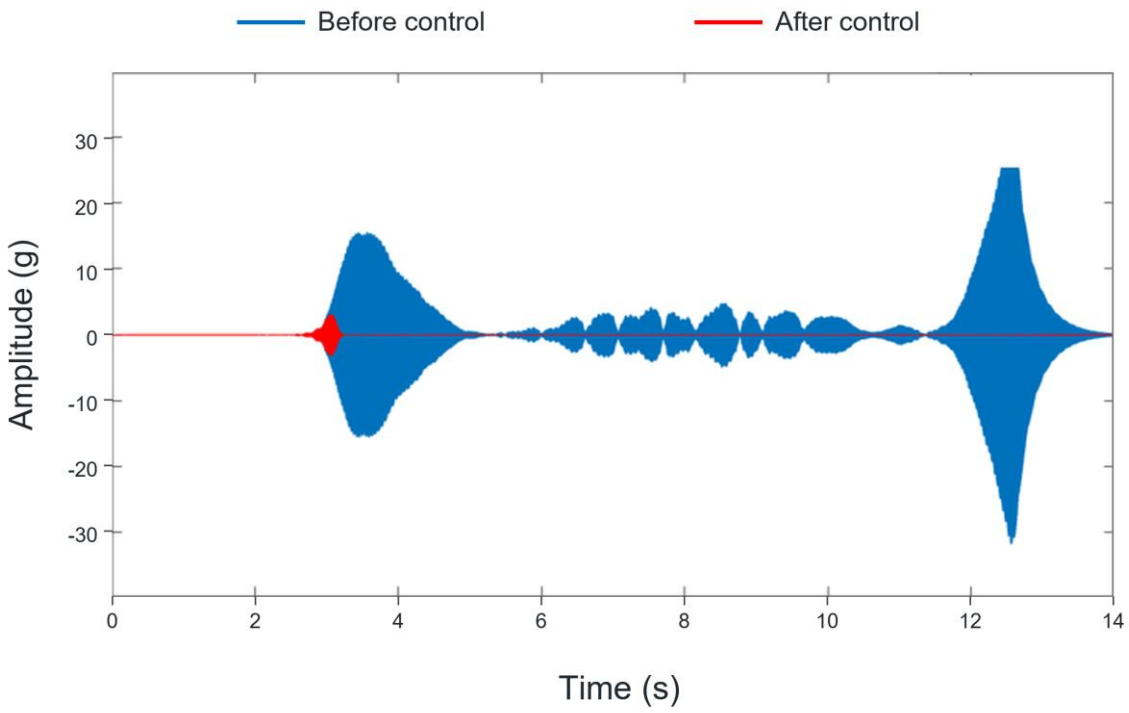


Fig. 10 Example of the measured signal before and after offline FxLMS control

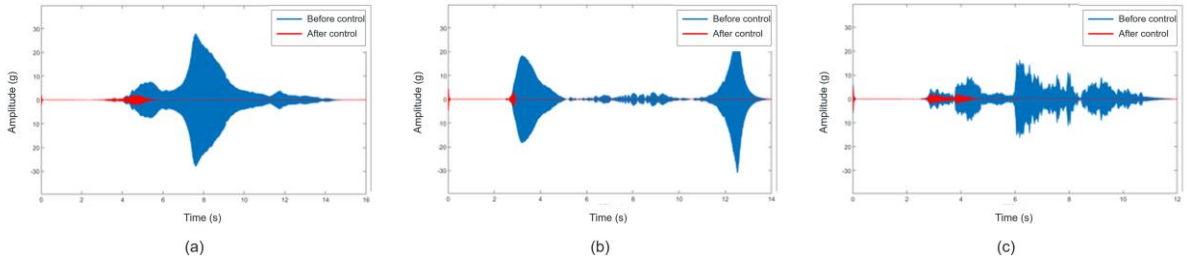


Fig. 11 Offline suppression results for measured milling signals: (a) 5000 r/min; (b) 6000 r/min; (c) 7000 r/min

The target-band vibration packets contract after control, and the dominant spectral components decrease without obvious enlargement of non-target bands in the displayed examples. The short transient near control onset reflects adaptive-weight convergence and should not be interpreted as steady-state performance. The measured-signal simulations demonstrate applicability to the available signal records, but they remain offline evaluations: they do not replace real-time machining tests and do not prove that a fixed secondary-path estimate covers every future spindle speed or structural configuration.

4.3 Comparative milling tests

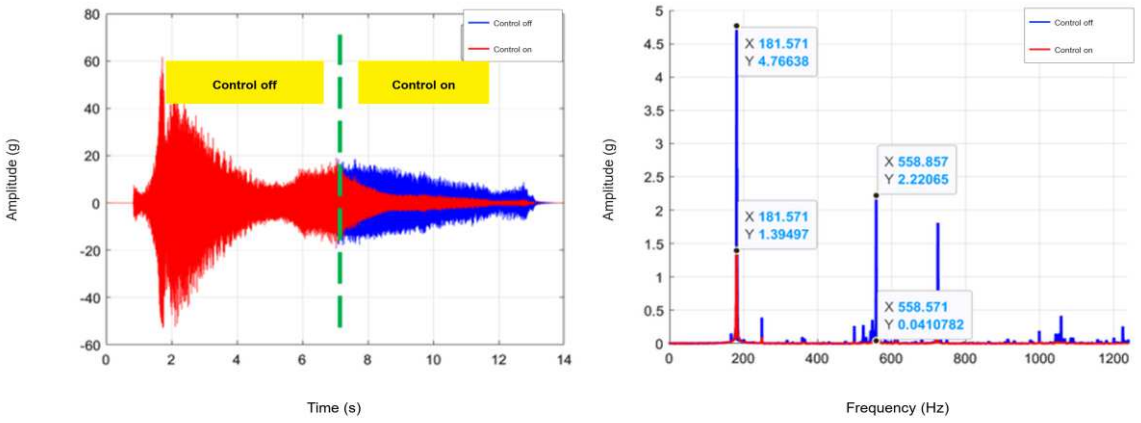
Comparative milling tests are performed on the platform shown in Fig. 12. The same workpiece, tool, sensing chain, and machining path are maintained within each condition. The spindle speed is the main varied parameter; cutting depth, cutting width, and feed per tooth remain fixed as listed in Table 3. For each speed, the controller is switched from an uncontrolled interval to an active-control interval during the same cutting run. The resulting acceleration response therefore represents a within-run transition rather than two unrelated tests. Surface roughness Ra is measured in the corresponding uncontrolled and controlled regions to assess whether vibration reduction is accompanied by improved surface quality.



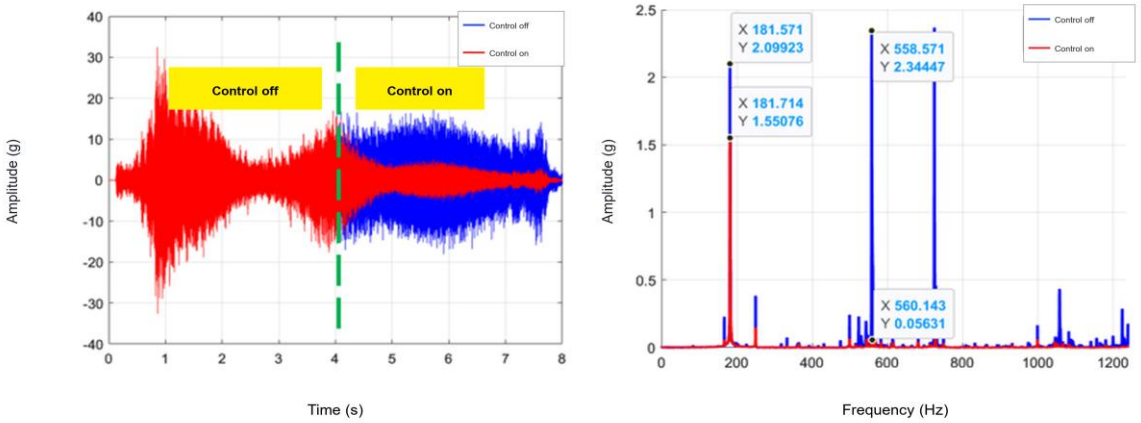
Fig. 12 Milling-test arrangement on the NINGQING machining centre

Table 3 Milling parameters for the single-factor spindle-speed tests

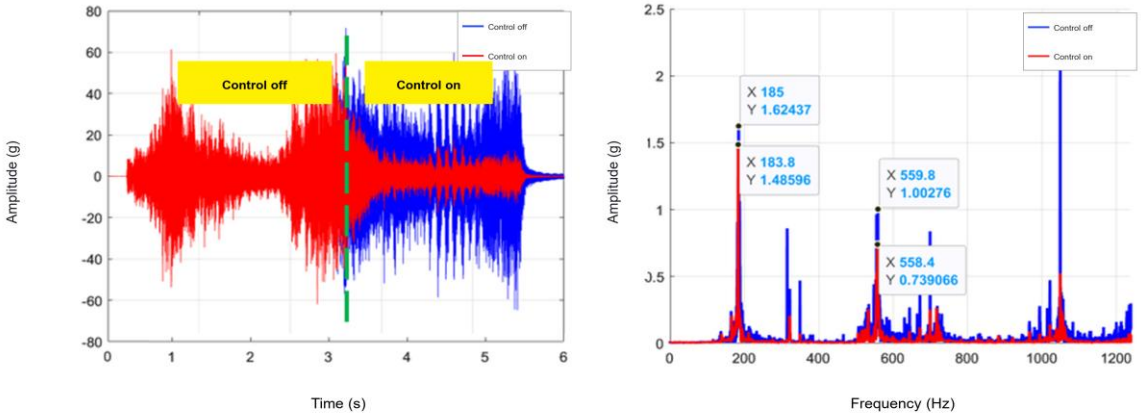
Test	Spindle speed (r/min)	Axial depth (mm)	Radial width (mm)	Feed per tooth (mm/tooth)
1	4000	0.5	2	0.1
2	7000	0.5	2	0.1
3	10000	0.5	2	0.1



(a) 4000 r/min



(b) 7000 r/min



(c) 10000 r/min

Fig. 13 Acceleration responses before and after controller activation: (a) 4000 r/min; (b) 7000 r/min; (c) 10000 r/min

At 4000 r/min, the vibration amplitude decreases from approximately 20 g to 5 g, corresponding to a reduction of about 75%. The peaks at 181.571 and 558.857 Hz decrease from 4.766 and 2.221 to 1.395 and 0.041, respectively. At 7000 r/min, the vibration amplitude decreases from approximately 15 g to 5 g (66.7%), and the two reported peak amplitudes decrease from 2.099 and 2.344 to 1.551 and 0.056. At 10000 r/min, the vibration amplitude decreases from approximately 40 g to below 20 g (about 50%); the reported peaks near 185 and 559.8 Hz decrease from 1.624 and 1.003 to 1.486 and 0.739. The weaker high-speed improvement indicates sensitivity to stronger tool–workpiece–machine coupling, fixed secondary-path-model error, and finite adaptation time.

Table 4 Surface-roughness comparison at three spindle speeds

Spindle speed (r/min)	Uncontrolled Ra (μm)	FxLMS-controlled Ra (μm)	Reduction
4000	3.2	1.1	65.6%
7000	2.8	1.3	53.6%
10000	4.5	3.8	15.6%

Surface roughness follows the same speed-dependent trend as vibration suppression. Ra decreases by 65.6%, 53.6%, and 15.6% at 4000, 7000, and 10000 r/min, respectively. The consistent direction of change supports a link between reduced target-band vibration and improved machined-surface quality on the investigated platform. The high-speed result also defines an important boundary: a fixed secondary-path estimate and parameter set do not fully compensate for all changes in structural and machining dynamics.

5 Conclusions

This study developed a secondary-path-compensated FxLMS method for active chatter suppression in thin-plate milling. The work was motivated by the mismatch between the direct-gradient assumption of conventional LMS and the actual controller–actuator–plate–sensor path. The following conclusions are drawn within the limits of the investigated platform and parameters:

- The physical secondary path must be included in the adaptive update because its gain, phase, and delay change the relationship between controller output and measured acceleration. A compact control-force-to-acceleration estimate provides a practical target-band model for FxLMS prefiltering.
- In simulation under identical conditions with a 0.8 ms delay, conventional LMS reduced steady-state RMS by only 8.1% and amplified the 558.857 Hz component. FxLMS reduced RMS by 82.9% and simultaneously attenuated the 181.571 and 558.857 Hz components by 91.6% and 69.8%, demonstrating correction of the multi-frequency gradient mismatch under the modelled conditions.
- Measured-signal offline simulations and milling tests supported the applicability of the method beyond the idealised disturbance. At 4000, 7000, and 10000 r/min, vibration amplitude decreased by approximately 75.0%, 66.7%, and 50.0%, while Ra decreased by 65.6%, 53.6%, and 15.6%.
- The declining benefit at 10000 r/min indicates the boundary of a fixed secondary-path estimate and a single controller parameter set. Future work should investigate online or scheduled secondary-path updating, broader multimodal models, and robustness under larger changes in cutting load and structural boundary conditions.

References

[1] Su YH, Hu Y. Research progress on milling technology for aerospace aluminium-alloy thin-walled parts. Equipment Manufacturing Technology. 2024;(10):174–178. [in Chinese]

[2] Wang YH, Wang M. Research progress on chatter-control technologies in metal cutting. Journal of Mechanical Engineering. 2010;46(7):166–174. [in Chinese]

[3] Wu Y, He Y, Song HR, et al. Review of cutting-chatter control for thin-walled parts. Manufacturing Technology & Machine Tool. 2021;(11):49–53. [in Chinese]

[4] Yang K, Huang LX. Review of research progress on cutting chatter. Chinese Journal of Applied Mechanics. 2019;36(6):1464–1470, 1528. [in Chinese]

[5] Li C, Zhang J, Tian H, et al. Real-time milling-chatter monitoring based on vibration-signal energy ratio and amplitude standard deviation. Journal of Mechanical Engineering. 2024;60(14):11–23. [in Chinese]

[6] Kolluru K, Axinte D. Novel ancillary device for minimising machining vibrations in thin wall assemblies. International Journal of Machine Tools and Manufacture. 2014;85:79–86.

[7] Chen TT, Li DJ, Zhang SY, et al. Design and testing of a viscous damper for thin-walled parts. Journal of Vibration and Shock. 2022;41(7):68–73. [in Chinese]

[8] Liu HB, Zhang HZ, Wang CX, et al. Suppression of milling vibration in thin-walled parts using added mass and eddy-current damping. Aeronautical Manufacturing Technology. 2023;66(3):53–60. [in Chinese]

[9] Jiang X, Zhao G, Lu W. Vibration suppression of complex thin-walled workpiece based on magnetorheological fixture. The International Journal of Advanced Manufacturing Technology. 2020;106(3–4):1043–1055.

[10] Yang YQ, Xie RC, Xu DD. Milling-chatter suppression of thin-walled parts using a rotating variable-stiffness damper. Journal of Vibration and Shock. 2018;37(2):72–75, 84. [in Chinese]

[11] Qiu ZC, Ma B. Adaptive resonant vibration control of a piezoelectric flexible plate implementing filtered-X LMS algorithm. International Journal of Acoustics and Vibration. 2014;19(4):224–239. https://doi.org/10.20855/ijav.2014.19.4355.

[12] Kaliński KJ, Galewski MA. Vibration surveillance supported by hardware-in-the-loop simulation in milling flexible workpieces. Mechatronics. 2014;24(8):1071–1082.

[13] Cao HR, Li DH, Liu JX, et al. Fuzzy control of high-speed milling chatter for an intelligent spindle. Journal of Mechanical Engineering. 2021;57(13):55–62. [in Chinese]

[14] Rashid A, Nicolescu CM. Active vibration control in palletised workholding system for milling. International Journal of Machine Tools and Manufacture. 2006;46(12–13):1626–1636. https://doi.org/10.1016/j.ijmachtools.2005.08.020.

[15] Du J, Long X. Chatter suppression for milling of thin-walled workpieces based on active modal control. Journal of Manufacturing Processes. 2022;84:1042–1053. https://doi.org/10.1016/j.jmapro.2022.10.061.

[16] Ren JB, Sun GZ, Chen B, et al. Online milling-chatter monitoring based on multiscale permutation entropy. Journal of Mechanical Engineering. 2015;51(9):206–212. [in Chinese]

[17] Schmitz TL, Medicus K, Dutterer B. Exploring once-per-revolution audio signal variance as a chatter indicator. Machining Science and Technology. 2002;6(2):215–233.

[18] Zhang Z, Liu CY, Zhang J, et al. Milling-chatter identification based on characteristic-frequency groups. Modular Machine Tool & Automatic Manufacturing Technique. 2018;(9):24–26, 29. [in Chinese]

[19] Liu CF, Zhu LD, Ni CB. The chatter identification in end milling based on combining EMD and WPD. The International Journal of Advanced Manufacturing Technology. 2017;91(9–12):3339–3348.

[20] Jing X, Yang H, Song X, et al. A novel chatter detection method in micro-milling process using wavelet packet entropy. The International Journal of Advanced Manufacturing Technology. 2024;131(9–10):5289–5303.

[21] Mou WP, Zhu SW, Jiang ZX, et al. Vibration signal-based chatter identification for milling of thin-walled structure. Chinese Journal of Aeronautics. 2022;35(1):204–214.

[22] Kuo SM, Morgan DR. Active noise control: a tutorial review. Proceedings of the IEEE. 1999;87(6):943–975. https://doi.org/10.1109/5.763310.

[23] Bjarnason E. Analysis of the filtered-X LMS algorithm. IEEE Transactions on Speech and Audio Processing. 1995;3(6):504–514. https://doi.org/10.1109/89.482218.

[24] Li W, Yang Z, Li K, et al. Hybrid feedback PID-FxLMS algorithm for active vibration control of cantilever beam with piezoelectric stack actuator. Journal of Sound and Vibration. 2021;509:116243. https://doi.org/10.1016/j.jsv.2021.116243.

[25] Cai M. Data-driven chatter identification and active-control methods for thin-walled workpiece milling [dissertation]. Nanjing: Nanjing University of Aeronautics and Astronautics; 2025. [in Chinese]

Statements and Declarations

Funding: This work was supported by the Fundamental Research Funds for the Central Universities (Grant No. NG2024013).

Data availability: The data supporting the findings of this study are not publicly available due to project and partner confidentiality restrictions.

Competing interests: The authors declare that they have no relevant financial or non-financial interests to disclose.

Author contributions: Zicheng Wang performed experimental data acquisition, processing, analysis and validation, refined the control approach, and drafted the manuscript. Cheng Wang assisted with the experimental work and validation. Benchi Zhu and Wenbo He provided methodological guidance and research assistance. Mingjie Cai designed and built the experimental platform and selected the initial control algorithm. Guolong Zhao reviewed the manuscript and guided its structure and argumentation. Yinfei Yang supervised the project, secured funding, established the research direction, and reviewed the experimental results and control approach. All authors approved the manuscript for submission.

Ethics approval: Not applicable to the reported mechanical-engineering experiments.

Consent to participate: Not applicable.

Consent for publication: Not applicable.

Use of AI-assisted tools: During manuscript preparation, the authors used ChatGPT (OpenAI) to assist with Chinese-to-English translation, language editing, and organisation of the presentation. The authors reviewed and revised the resulting text and take responsibility for the final manuscript.